Rapid Communications

Measuring hole *g*-factor anisotropies using transverse magnetic focusing

Samuel Bladwell and Oleg P. Sushkov
School of Physics, University of New South Wales, Sydney 2052, Australia

(Received 21 January 2019; published 5 February 2019)

Recent theoretical and experimental results from quasi-one-dimensional heavy-hole systems have suggested that heavy-hole gases have a strongly anisotropic g factor. In this theoretical work, we propose a method for measuring this anisotropy using transverse magnetic focusing (TMF). We demonstrate that for experimentally accessible fields, the g-factor anisotropy leads to a relative variation in the characteristic of spin splitting of the TMF spectrum which allows for the measurement of the anisotropy of the g factor. We show that this variation is insensitive to additional spin-orbit interactions, and is resolvable with current devices.

DOI: 10.1103/PhysRevB.99.081401

The strength of the coupling of an electron to a magnetic field in free space is defined by the Bohr magneton μ_B and the electron g factor. Like free electrons, quasiparticles in condensed matter systems couple to an applied magnetic field, however, the form and magnitude of the g factor is strongly influenced by the surrounding material. The "renormalization" of the g factor can lead to effective g factors for charge carriers in semiconductors that are orders of magnitude larger than the free-space value. With such large values, an applied magnetic field can result in a significant change to transport properties, even in relatively weak magnetic fields. This effect persists in reduced dimensional systems, and can be enhanced or suppressed, and develop asymmetries depending on the confinement. In low-dimensional hole systems additional kinematic structures are possible, due to the holes' angular momentum being $J = 3/2$, with the Zeeman interaction in heavy-hole systems depending on both momentum and in-plane magnetic field [1,2]. Recent experimental and theoretical results suggest a strongly anisotropic in-plane g factor for two- and quasi-one-dimensional heavy-hole systems [3,4].

Measuring the g-factor anisotropy is difficult with typical transport techniques. For instance, magnetic (Shubnikov–de Haas) oscillations measure the total size of the Fermi surface and therefore have no first-order dependence on the anisotropy. Instead, Shubnikov–de Haas oscillations measure the total Fermi surface area. In this Rapid Communication, we propose a method to measure the relative g factors in hole systems, based around transverse magnetic focusing (TMF), which has a long history of use in the measurement of the shape of the Fermi surface in both metals and semiconductors (see Fig. 1) [5–9]. When employed in systems with strong spin-orbit coupling, the first magnetic focusing peak is spin split, resulting in a "double" focusing spectrum [10–15]. This spin splitting can be directly translated to the strength of the spin-orbit interaction. We make use of this feature, combined with a unique dependence on magnetic field rotations in TMF resulting from the anisotropy in the hole g factor, to determine the magnitude of the anisotropy. We then demonstrate that the effect is robust in the presence of surface or bulk inversion asymmetry that is weaker that the Zeeman interaction due to the in-plane field, and provides a straightforward method of determining g_1 and g_2.

We begin with a kinematic structure leading to this g-factor anisotropy in two-dimensional hole systems. Holes have a total angular momentum of $J = 3/2$. At $k = 0$, there are four degenerate states, typically denoted as "light," $\pm 1/2$, and "heavy," $\pm 3/2$, holes due to the difference in effective mass. When confined to two dimensions only the heavy holes lie below the chemical potential. Coupling $J_z = 3/2$ to $J_z = -3/2$ requires $J_\pm^3$, which is obtained with the combined action of the Luttinger term $(\mathbf{P}\cdot\mathbf{J})^2$ [1,16] and Zeeman interaction $\mathbf{B}\cdot\mathbf{J}$. Two kinematic structures are possible, $P_+^2 B_+ J_-^3$, or $P_+^4 B_- J_-^3$. Since only the heavy holes lie below the chemical potential, it is convenient to work in the subspace $\pm 3/2$, spanned by the Pauli matrices, with $J_\pm^3 \to \sigma_\pm$. The kinematic structure is then

$$\mathcal{H}_1 = \frac{g_1\mu_B}{2}(B_+ p_+^2\sigma_- + B_- p_-^2\sigma_+) \tag{1}$$

for the g_1 interaction and

$$\mathcal{H}_2 = \frac{g_2\mu_B}{2}(B_- p_+^4\sigma_- + B_+ p_-^4\sigma_+) \tag{2}$$

for the g_2 interaction. Here, $p_\pm = p_x \pm i p_y$ and $\sigma_\pm = \sigma_x + i\sigma_y$. Due to the momentum dependence of the interactions, the coefficients g_1 and g_2 are not dimensionless. For the following analytical calculations it is useful to consider the dimensionless coefficients,

$$\tilde{g}_1 = g_1 k_F^2, \quad \tilde{g}_2 = g_2 k_F^4, \tag{3}$$

where $k_F = \sqrt{2m\varepsilon_F}$ is the Fermi momentum, and ε_F is the Fermi energy. Importantly, recent theoretical and experimental work has shown that at experimental accessible densities, $\tilde{g}_2$ can be comparable to $\tilde{g}_1$ [3,4].

The Hamiltonian for a hole system subject to these two respective Zeeman interactions due to an in-plane magnetic field, and some significantly weaker transverse focusing field is

$$\begin{aligned}\mathcal{H} &= \frac{\hat{\boldsymbol{\pi}}^2}{2m} + \mathcal{H}_1 + \mathcal{H}_2 + \frac{g_z\mu_B}{2}B_z\sigma_z \\ &= \frac{\hat{\boldsymbol{\pi}}^2}{2m} + \mathcal{B}(\hat{\boldsymbol{\pi}})\cdot\boldsymbol{\sigma}, \\ \hat{\boldsymbol{\pi}} &= \hat{\boldsymbol{p}} - e\boldsymbol{A},\end{aligned} \tag{4}$$

 ©2019 American Physical Society

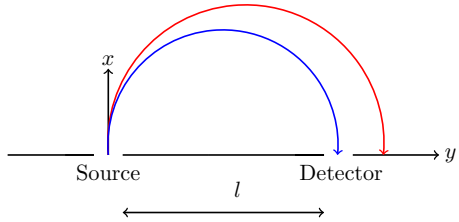

FIG. 1. Magnetic focusing setup, with focusing length l. The source and detector in hole systems are typically quantum point contacts (QPCs).

where $\boldsymbol{A}$ is the vector potential. The equations of motion are

$$\dot{\hat{\boldsymbol{\pi}}} = i[\mathcal{H}, \hat{\boldsymbol{\pi}}] = m\omega_c \hat{\mathbf{v}} \times \mathbf{n},$$
$$\dot{\boldsymbol{\sigma}} = i[\mathcal{H}, \boldsymbol{\sigma}] = -\mathcal{B}(\hat{\boldsymbol{\pi}}) \times \boldsymbol{\sigma}, \tag{5}$$

where $\omega_c = eB_z/m$. Solving these equations of motion requires some approximation of spin dynamics. In the case of TMF, the appropriate approximation for the resolution of a double focusing peak is adiabatic spin dynamics, where the spin follows the instantaneous effective magnetic field $\langle\boldsymbol{\sigma}\rangle = s\mathcal{B}/|\mathcal{B}|$, where $s = \pm 1$ is a pseudoscalar defining the spin projection [11]. The resulting semiclassical equation is obtained using the method of Refs. [17,18],

$$\mathbf{r}(\theta(t)) = \frac{\boldsymbol{\pi}(\theta(t)) \times \mathbf{n}}{eB_z} - \frac{\boldsymbol{\pi}(\theta(0)) \times \mathbf{n}}{eB_z}, \tag{6}$$

where the momentum $\boldsymbol{\pi}$ depends on the spin state of the hole, and $\theta(t)$ is the polar (running) angle and is a function of time. Physically, this corresponds to the classical cyclotron motion of quasiparticles with different cyclotron radii depending on the spin projection. We present both cyclotron orbits and spin orientations in Fig. 2.

To explore the dynamics analytically, we consider the following approximation for the spin-split momentum $\boldsymbol{\pi}$,

$$\boldsymbol{\pi} = \hbar k_{F,s}[\cos\theta(t), \sin\theta(t), 0],$$
$$k_{F,s} = k_F\left(1 + \frac{s|\mathcal{B}|}{2\varepsilon_F}\right), \tag{7}$$

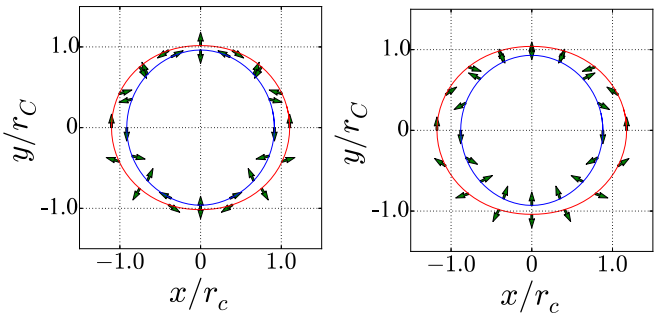

FIG. 2. Cyclotron orbits for spin down (red) and up (blue) with the spin ($\langle\boldsymbol{\sigma}\rangle$) orientation in the adiabatic limit. The left panel has $\tilde{g}_2/\tilde{g}_1 = 0.5$, while the right panel has $\tilde{g}_1/\tilde{g}_2 = 0.5$. We note that while the Fermi surfaces have a nearly identical shape, due to the different momentum dependence of the two interactions, the spin dynamics are qualitatively different.

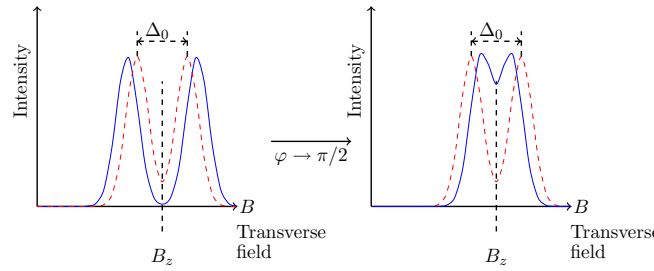

FIG. 3. Cartoon of the variation in the focusing splitting. The red dashed curve is the TMF spectrum without any g-factor asymmetry, with splitting magnitude Δ_0, with $\Delta_0 = \tilde{g}_1\mu_B B_{||}/\varepsilon_F$. The blue curve is the TMF spectrum, including the g-factor anisotropy, with $\varphi = 0$ for the left panel, and $\varphi = \pi/2$ for the right panel. The focusing field without spin splitting, $B_z = 2k_F/el$, is marked with a dashed black line.

where the total effective magnetic field is

$$|\mathcal{B}| = \mu_B B_{||}\sqrt{\tilde{g}_1^2 + \tilde{g}_2^2 + 2\tilde{g}_1\tilde{g}_2\cos(2\theta - 2\varphi)} \tag{8}$$

with an in-plane field angle φ, and

$$\boldsymbol{B} = (B_{||}\cos\varphi, B_{||}\sin\varphi, B_z) \tag{9}$$

being the magnetic field applied to the sample. To satisfy the requirement for adiabatic spin dynamics, we need to ensure that the magnetic field remains sufficiently large. If $\tilde{g}_1 > \tilde{g}_2$, the approximate condition of adiabatic spin dynamics is

$$|\mathcal{B}| \gg \frac{1}{|\mathcal{B}|}\frac{\partial\mathcal{B}}{\partial t} \sim 2\omega_c, \tag{10}$$

where the factor of 2 comes for the two rotations of the spin-orbit field for each rotation in momentum space (see Fig. 2). In this adiabatic regime, the classical focusing peak where interference effects are neglected corresponds to an injection angle of $\theta = 0$ [19]. The focusing length l from Eqs. (6) and (8) is

$$l = y(\theta = \pi) \approx \frac{\hbar k_{F,s}(\theta = 0) + \hbar k_{F,s}(\theta = \pi)}{eB_z}, \tag{11}$$

which is analogous to the case of classical TMF in metals [6]. We have cast the above result in terms of spatial variation of the peaks; in TMF the detector and collector are fixed, and the focusing field B_z is varied instead,

$$B_z \approx \frac{\hbar k_{F,s}(\theta = 0) + \hbar k_{F,s}(\theta = \pi)}{el}. \tag{12}$$

For $2\omega_c \ll |\mathcal{B}| \ll \varepsilon_F$, using Eqs. (12) and (8),

$$\frac{\delta B_z}{B_z} \approx \frac{k_+(\varphi) - k_-(\varphi)}{k_F}, \tag{13}$$

where δB_z denotes the splitting between the spin-split focusing peaks. Figure 1 corresponds to a fixed B_z and a varied focusing length l; in a real experiment, l is fixed and B_z is varied (see Fig. 3).

We are now in a position to explore the angular dependence of the in-plane field response in the TMF spectrum. We consider the case of a relatively short focusing length, of $l = 1000$ nm, with a hole density $n = 1.65 \times 10^{11}$ cm^{-2}. Let us start with the case where all other spin-orbit interactions have been tuned to be small. For quantum wells grown along

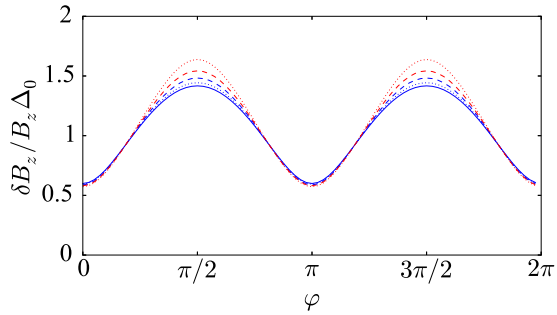

FIG. 4. The field angle dependence of the first focusing peak splitting, with increasing in-plane magnetic field, from 1 to 3.5 T, with $\tilde{g}_2 = 1$ and $\tilde{g}_1 = -2.5$. The deviation from Eq. (14) is the result of the nonparabolic terms in the dispersion.

high-symmetry axes, this is a reasonable approximation. For the case where $\tilde{g}_1 \gg \tilde{g}_2$, by expanding in terms of $\tilde{g}_2/\tilde{g}_1$, we obtain the following approximate analytical expression for the angular dependence,

$$\frac{\delta B_z}{B_z \Delta_0} \approx \left(1 + \frac{\tilde{g}_2}{\tilde{g}_1}\cos(2\varphi)\right), \tag{14}$$

where we have introduced the dimensionless splitting $\Delta_0 = \tilde{g}_1 \mu_B B_{||}/\varepsilon_F$. In Fig. 4 we plot the fractional focusing field splitting $\delta B_z/B_z\Delta_0$ as a function of the in-plane field angle φ. Here, $\tilde{g}_1 = -2.5$ and $\tilde{g}_2 = 1$. For GaAs quantum wells, $|\tilde{g}_1|$, $|\tilde{g}_2| < 3$, dependent on the manner of the confinement [4].

In practice, other spin-orbit interactions due to bulk and surface inversion symmetry may not be small. To examine the influence of additional spin-orbit interactions we consider a Rashba spin-orbit interaction, $\mathcal{H}_R = i\gamma_R p_+^3 \sigma_-/2 + \text{H.c.}$, resulting from an asymmetric confining potential. The Rashba induces a spin splitting in the hole gas of $\Delta_R = \gamma_3 \hbar^3 k_F^3/\varepsilon_F$. We include the Rashba term in the Hamiltonian, Eq. (5), and use the aforementioned method to determine the variation in the focusing field. In Fig. 4 we present the response to in-plane magnetic field rotations, with varying strength of the Rashba spin-orbit interaction. Provided $\Delta_R < \tilde{g}_1 \mu_B B_{||}/\varepsilon_F$ and $\Delta_R < \tilde{g}_2 \mu_B B_{||}/\varepsilon_F$, there is minimal variation in the magnetic focusing field splitting δB_z. In general, spin-orbit interactions which are odd in momentum such as the Dresselhaus and Rashba interactions will only weakly perturb the variation in the TMF peak spacing.

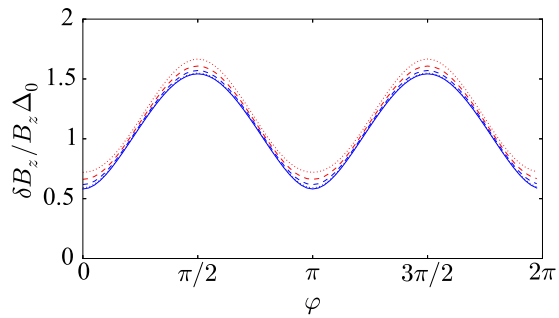

FIG. 5. Relative focusing field splitting as a function of the in-plane magnetic field angle φ with $B_{||} = 2.5$ T, $\tilde{g}_1 = -2.5$, $\tilde{g}_2 = 1$. Here, we vary the strength of the Rashba interaction Δ_R in the range $0 < \Delta_R < 0.1\epsilon_F$. The maximum value is $\Delta_R \sim 0.2$ meV.

The measurement of $\tilde{g}_2/\tilde{g}_1$ depends only on the classical focusing field, and is therefore independent of the source and detector. However, the effect must be larger that the spread of the focusing peaks to be observed, $\delta B_z/B_z \geqslant B_{\text{FWHM}}/B_z$, where B_{FWHM} is the full width at half maximum of the focusing peak. Recent hole experiments with spin splitting induced via a large Rashba-type interaction have $B_{\text{FWHM}} \sim 0.02$ T [10], giving a ratio of $B_{\text{FWHM}}/B_z \sim 0.1$. To make a direct comparison between this and our results, we consider an in-plane field of $B_{||} = 3.5$ T and $\tilde{g}_1 = -2.5$, with $\Delta_0 \approx 0.2$. Comparing to Fig. 4, the minimum value at $\theta = \pi$ corresponds to an effective splitting $\delta B_z/B_z > 0.1$. Hence the two peaks are resolvable over the full range of φ at $B_{||} = 3.5$ T.

Finally, we turn our attention to the assumption of adiabatic spin dynamics that we have employed in preceding calculations. As has been noted, $2\omega_c \ll |\mathcal{B}_{\text{min}}|$. The minimum value of $\mathcal{B}$,

$$|\mathcal{B}_{\text{min}}| = (|\tilde{g}_1| - |\tilde{g}_2|)\mu_B B_{||}, \tag{15}$$

which results in the following condition,

$$4\frac{m}{m^*}\frac{B_z}{B_{||}} < |\tilde{g}_1| - |\tilde{g}_2| \approx 1. \tag{16}$$

The fraction $B_z/B_{||}$ is the ratio between the in-plane field, and the focusing field, while m^* is the effective mass. For a typical device, $B_z \sim 0.1$ T, while $B_{||}$ can be several tesla, and in quantum wells, $m^* \sim 0.2m$. We can compare this to some recent results in GaAs heavy-hole quantum wells. The commensurate criterion to (16) is

$$3\omega_c < \Delta_R, \tag{17}$$

where Δ_R is the strength of the Rashba splitting, $\Delta_R \sim 0.2\varepsilon_F$, which can be converted to an expression in terms of the Fermi momentum k_F and focusing length l,

$$\frac{12}{k_F l} < \Delta_R. \tag{18}$$

For this Rashba hole system, $k_F l \sim 100$, so $\Delta_R k_F l/12 \sim 1/2$, while the two spin-split peaks are still clearly observable. Comparing this to Eq. (16), $B_{||} \sim 4$ T is sufficient to satisfy this condition. Taken together with considerations of the spread of the focusing peak, we can conclude that it is possible to measure anisotropies in the in-plane g factor in hole systems using TMF.

In summary, we have shown TMF can be used to determine the relative magnitude of $\tilde{g}_1$ and $\tilde{g}_2$, via the unique dependence on the in-plane magnetic field angle φ. Furthermore, this dependence is robust with the addition of residual spin-orbit interactions. Based on results from TMF in heavy-hole gases, variation of the focusing field is significantly larger than the broadening due to both scattering and the finite size of injectors and detectors at experimentally accessible in-plane fields.

This work was supported by the Australian Research Council Centre of Excellence in Future Low-Energy Electronics Technologies (Project No. CE170100039) and funded by the Australian Government. The authors would like to thank D. Miserev for his valuable discussions.

[1] R. Winkler, *Spin-Orbit Coupling Effects in Two-Dimensional Electron and Hole Systems*, Springer Tracts in Modern Physics Vol. 191 (Springer, Berlin, Heidelberg, 2003).
[2] T. Li, L. A. Yeoh, A. Srinivasan, O. Klochan, D. A. Ritchie, M. Y. Simmons, O. P. Sushkov, and A. R. Hamilton, Phys. Rev. B **93**, 205424 (2016).
[3] D. S. Miserev and O. P. Sushkov, Phys. Rev. B **95**, 085431 (2017).
[4] D. S. Miserev, A. Srinivasan, O. A. Tkachenko, V. A. Tkachenko, I. Farrer, D. A. Ritchie, A. R. Hamilton, and O. P. Sushkov, Phys. Rev. Lett. **119**, 116803 (2017).
[5] Yu. V. Sharvin, Zh. Eksp. Teor. Fiz. **48**, 984 (1965) [Sov. Phys. JETP **21**, 655 (1965)].
[6] Yu. V. Sharvin and L. M. Fisher, Pis'ma Zh. Eksp. Teor. Fiz. **1**, 54 (1965) [JETP Lett. **1**, 152 (1965)].
[7] V. S. Tsoi, Sov. Phys. JETP Lett. **19**, 70 (1974).
[8] V. S. Tsoi, J. Bass, and P. Wyder, Rev. Mod. Phys. **71**, 1641 (1999).
[9] H. van Houten, C. W. J. Beenakker, J. G. Williamson, M. E. I. Broekaart, P. H. M. van Loosdrecht, B. J. van Wees, J. E. Mooij, C. T. Foxon, and J. J. Harris, Phys. Rev. B **39**, 8556 (1989).
[10] L. P. Rokhinson, V. Larkina, Y. B. Lyanda-Geller, L. N. Pfeiffer, and K. W. West, Phys. Rev. Lett. **93**, 146601 (2004).
[11] U. Zülicke, J. Bolte, and R. Winkler, New J. Phys. **9**, 355 (2007).
[12] G. Usaj and C. A. Balseiro, Phys. Rev. B **70**, 041301 (2004).
[13] A. Reynoso, G. Usaj, and C. A. Balseiro, Phys. Rev. B **75**, 085321 (2007).
[14] J. Schliemann, Phys. Rev. B **77**, 125303 (2008).
[15] A. Kormányos, Phys. Rev. B **82**, 155316 (2010).
[16] J. M. Luttinger and W. Kohn, Phys. Rev. **97**, 869 (1955).
[17] S. Bladwell and O. Sushkov, Phys. Rev. B **92**, 235416 (2015).
[18] S. Bladwell and O. Sushkov, Phys. Rev. B **95**, 159901 (2017).
[19] S. Bladwell and O. Sushkov, Phys. Rev. B **96**, 035413 (2017).